Title

Faraday instability-based micro droplet ejection for inhalation drug delivery.

Journal

TECHNOLOGY, 2(1)

ISSN

2339-5478

Authors

Tsai, C

Mao, R

Lin, S

et al.

Publication Date

2014-03-01

DOI

10.1142/S233954781450006X

Peer reviewed

ARTICLE

TECHNOLOGY

Faraday instability-based micro droplet ejection for inhalation drug delivery

C.S. Tsai[1,3], R.W. Mao[1], S.K. Lin[1], Y. Zhu[1] & S.C. Tsai[2]

We report here the technology and the underlying science of a new device for inhalation (pulmonary) drug delivery which is capable of fulfilling needs unmet by current commercial devices. The core of the new device is a centimeter-size clog-free silicon-based ultrasonic nozzle with multiple Fourier horns in resonance at megahertz (MHz) frequency. The dramatic resonance effect among the multiple horns and high growth rate of the MHz Faraday waves excited on a medicinal liquid layer together facilitate ejection of monodisperse droplets of desirable size range (2–5 μm) at low electrical drive power (<1.0 W). The small nozzle requiring low drive power has enabled realization of a pocket-size (8.6 × 5.6 × 1.5 cm^3) ultrasonic nebulizer. A variety of common pulmonary drugs have been nebulized using the pocket-size unit with desirable aerosol sizes and output rate. These results clearly provide proof-of-principle for the new device and confirm its potential for commercialization.

INNOVATION

Drugs designed to treat pulmonary diseases or for systemic absorption through the massive surface area of the lung require optimum particle sizes (1 to 6 μm). Current advanced commercial devices such as Omron, Pari eFlow, and Philips I-neb produce droplets or aerosols by a vibrating mesh. All these devices suffer from broad particle size (poly-disperse) distributions and lack of size control capability, and also are plagued by clogging of mesh orifices used.

Here we report a new delivery device that has demonstrated capability for control of particle size within the optimum size range at low drive power and freedom from clogging. The new device employs a novel silicon-based ultrasonic nozzle with multiple Fourier horns in resonance designed to operate based on the newly discovered phenomena of Faraday waves at the frequency range of 1 to 2.5 MHz. The superior performance and batch fabrication economy of the centimeter-size nozzles have paved the way for commercialization of the new device.

INTRODUCTION

Inhalation is an increasingly important route for non-invasive drug delivery for both systemic and local applications[1–5]. Control of particle (aerosols or droplets in air) size and output plays a critical role in the efficient and effective delivery of often expensive medications to the lung. Drugs designed to treat pulmonary diseases or for systemic absorption through the alveolar capillary bed require optimum particle sizes (1 to 6 μm) for effective delivery. Based on deposition of aerosol particles in human respiratory tract following a slow inhalation (250 mL/s air rate) and a 5-second hold[4,5], particles 1 to 4 μm (in aerodynamic diameter) deposit primarily in the alveolar region while particles 3 to 6 μm deposit in the airways. Particles larger than 6 μm deposit primarily in the mouth and throat. It is to be noted that respirable particles in the 1–4 μm range are optimal for alveolar deposition, but contain less drug than particles in the 2–5 μm range by 4 to 8 times per particle. With proper control of particle size, drugs ranging from small molecules such as pentamidine to large molecules such as insulin could be effectively delivered as aerosols via inhalation for systemic absorption or local treatment in airways and lung parenchyma[6–10].

Current commercial devices such as Misty-Neb, AeroEclipse, Omron, Pari eFlow, and Philips I-neb produce droplets or aerosols by compressed air, a vibrating piezoelectric plate together with a metallic mesh, or a vibrating mesh. As the examples (plots a and b) show in **Fig. 1A**, all these devices suffer from broad particle size (poly-disperse) distributions (with high geometrical standard deviation (GSD) >1.5), making it difficult to deliver sufficient drug of desirable sizes to targeted sites precisely and rapidly. Furthermore, the eFlow and I-neb which utilize vibrating mesh technology[11] and are considered the most advanced commercial devices suffer from clogging of the mesh orifices used[12]. Thus, delivery devices with control capability in particle size and less susceptibility to clogging are clearly needed for rapid administration at sufficient quantities of often expensive drugs such as agents to treat pulmonary hypertension and toxic inhalation agent antidotes[13,14]. Here we report a new delivery device that utilizes a silicon-based megahertz (MHz) multiple-Fourier horn ultrasonic nozzle (MFHUN) and temporal instability of Faraday waves[15,16] to fulfill the unmet needs. As plots c, d, and e of **Fig. 1A** show, by varying the drive frequency of the MFHUN from 1.0 to 2.5 MHz the new device was capable of controlling the particle sizes within the optimum size range (1 to 6 μm) with a much narrower size distribution.

The much narrower droplet size distribution achieved by the new device (MFHUN), compared to advanced commercial devices, is also

[1]Department of Electrical Engineering and Computer Science, [2]Department of Chemical Engineering and Materials Science, University of California, Irvine, CA 92697, USA. [3]Institute of Optoelectronics and Photonics, National Taiwan University, Taipei, Taiwan. Correspondence should be addressed to C.S.T. (cstsai@uci.edu).

Received 2 September 2013; accepted 9 January 2014; published online 28 February 2014; doi:10.1142/S233954781450006X

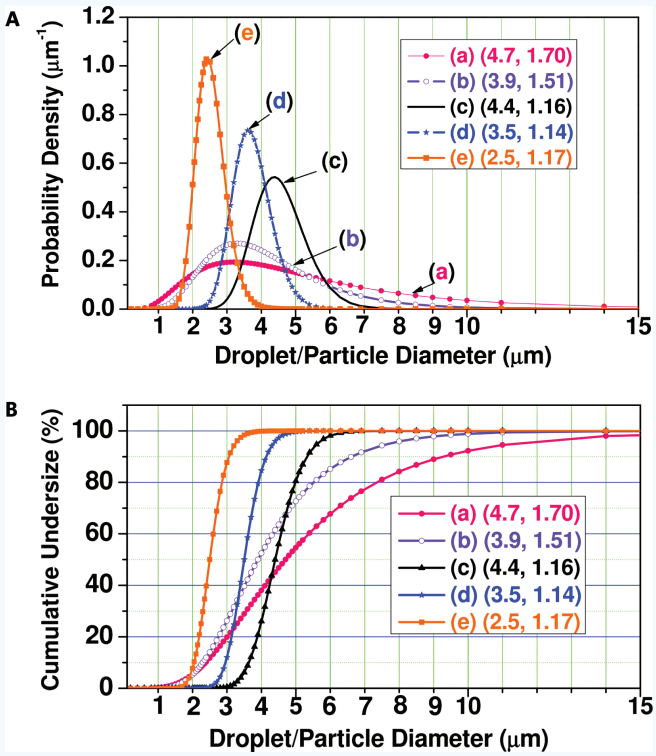

Figure 1 Comparison of (**A**) particle diameters and size distributions (MMAD/MMD μm, GSD), and (**B**) Cumulative undersize percentage between the commercial devices and the new device: (a) Philips I-neb[9], (b) Pari eFlow[8], (c) 1.0 MHz, (d) 1.5 MHz, and (e) 2.5 MHz. Note that MMAD for (a)–(b) and MMD for (c)–(e) stand for mass median aerodynamic diameter and mass median diameter, respectively; MMD and geometrical standard deviation (GSD) for the new device were obtained using Malvern/Spraytec particle sizer (Model #STP 5311); and GSD of 1.0 represents a single particle size and the closer the GSD to 1.0 the higher the monodispersity.

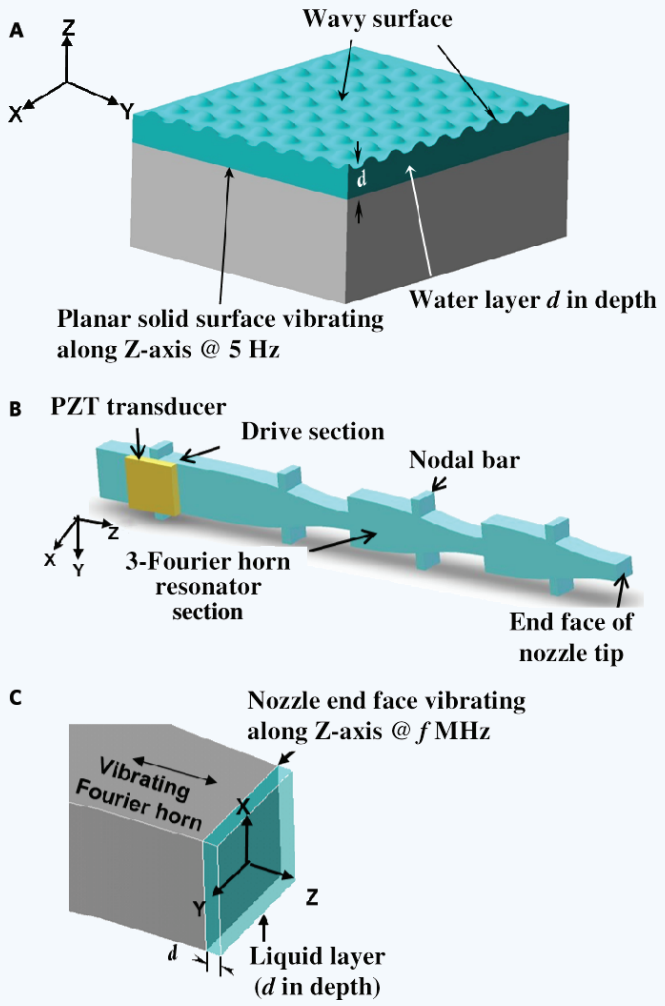

Figure 2 (**A**) Classical planar geometry for Faraday waves formation at low drive frequency (5 Hz). (**B**) 3-D architecture of the MHz multiple-Fourier horn ultrasonic nozzle. (**C**) Geometry of nozzle end face and planar liquid layer *d* in depth.

illustrated by its steeper cumulative undersize percentage curves as shown in **Fig. 1B**. Notably, plots c to e show that 100% or nearly 100% of droplets are smaller than 6 μm in diameter for the new device while plots a and b show only 66% and 85%, respectively, for the advanced commercial nebulizers. The much narrower droplet size distribution will have significant economic impact on lung deposition of drugs, especially of expensive drugs. For example, as shown in **Fig. 1A** the MMD of plot c obtained using the new device at 1 MHz drive frequency is similar to the MMAD of plot a obtained using one of the most advanced commercial nebulizers — the I-neb Adaptive Aerosol Delivery (AAD) System that delivers aerosol only during inspiration (i.e. breath actuation). However, as shown in plot c of **Fig. 1B** the narrower size distribution with a smaller GSD obtained by the former (1.16 versus 1.70) leads to a much greater respirable (inhaled) fraction (nearly 100% versus 66% with particle diameter <6 μm) than by the latter. Therefore, the inhaled dose delivered to the lung using the new device together with breath actuation should be much higher than the 60 ± 5% achievable using the I-neb AAD System[9]. Note that as presented in the final section of "Methods and Results", the capability of breath actuation with the pocket-size MFHUN unit has been demonstrated (**Fig. 6C**).

Faraday waves, also known as standing capillary waves, were first observed as wavy surface of a water layer resting on a solid surface subjected to perpendicular mechanical vibration, as depicted in **Fig. 2A**, at a very low drive (or forcing) frequency (5 Hz) by Faraday in 1831[17]. They were subsequently analyzed by Rayleigh in 1883[18] and many others[19]. Faraday instability, the underlying physical mechanism for Faraday wave formation and amplification, was studied[20–24] extensively based on the above classical planar geometry during the 1990s, and continued[25–29] in the 2000s, but mostly at very low drive frequency ranging from tens to thousands hertz (Hz). At such low drive frequencies, various standing-wave patterns were observed[25,30] when the mechanical vibration amplitude on the solid surface reached the onset threshold for Faraday wave formation. However, no droplet ejection (atomization) was described in the theoretical treatments of these earlier low-drive frequency studies. In the few reports on atomization at low drive frequencies, droplet ejection was found to take place only when the mechanical vibration amplitude on the solid surface was *much higher* than the onset threshold for Faraday wave formation. In stark contrast, our recent discovery as reported here using a novel device, silicon-based MHz MFHUN (see **Fig. 2B**), shows that at the much higher drive frequencies of MHz the onset threshold for Faraday wave formation is *much lower* and the mechanical vibration amplitude required for subsequent droplet ejection is *only slightly higher* than the onset threshold for Faraday wave formation[15]. These findings have also been verified by the rigorous theoretical treatment[31,32] summarized in the first section of "Methods and Results".

METHODS AND RESULTS

Linear theory on MHz Faraday wave instability for monodisperse micro droplet ejection

Classical model of planar liquid layer geometry

Figure 2C depicts the classical model geometry for theoretical study of Faraday instability reported here — a planar liquid layer of depth (d) resting on a planar solid surface mimicked by the end face of the silicon-based multiple-Fourier horn ultrasonic nozzle (MFHUN) that vibrates longitudinally along the nozzle axis (Z-axis) at the resonance frequency (f). The longitudinal vibration of the nozzle end face exerts a periodic pressure on the planar liquid layer. Faraday waves are formed on the free surface of the liquid layer when the peak vibration displacement of the nozzle end face (h) reaches the critical value or onset threshold (h_{cr}). The following theoretical treatment for the Faraday wave with amplitude $\xi(x, t)$ that represents the time-dependence displacement of the free liquid surface is based on mass-conservation and linearized Navier-Stokes equations for incompressible Newtonian liquids, such as water, with density ρ, surface tension σ, and kinematic viscosity ν[33].

Due to symmetry in the XY-plane, it is convenient to separate the coordinates into the perpendicular Z-direction and the XY-plane with x designating (x, y). First, we utilize Navier-Stokes equations and incompressibility condition, and apply the boundary conditions on the nozzle end face and the free liquid surface of the planar liquid layer geometry of **Fig. 2C**. The Navier-Stokes equations together with the Laplace's equation are solved by means of the Fourier transform in the horizontal coordinates (x) to result in the following equation for the temporal evolution of the amplitude ξ_k of the k^{th} mode Faraday waves for low-viscosity liquid such as water:

$$\partial_t^2 \xi_k(t) + 4\nu k^2 \partial_t \xi_k(t) + (\omega_k^2 + k g_e(t))\xi_k(t) = 0 \tag{1}$$

where the wave number (k) equals $2\pi/\lambda$ and $\omega_k^2 \equiv \sigma k^3/\rho$, and $g_e(t)$ is the external acceleration, equal to $h(2\pi f)^2\cos(2\pi f t)$. Finally, Eq. (1) is solved using the established technique for the k^{th} mode Faraday waves amplitude $\xi_k(x, t)$ in the most unstable region (the first tongue-like region) of the stability chart[15,34] and the result is given by Eq. (2).

Temporal instability of MHz Faraday waves and onset threshold for droplet ejection

The amplitude of the fastest growing k^{th} mode Faraday wave $\xi_k(t)$ in the most unstable region is obtained as follows:

$$\begin{aligned} \xi_k(t) &= \xi_0 e^{(\pi k f h - \beta)t} \sin(\pi f t - \pi/4), \\ \text{i.e. } \xi_k(t) &= \xi_0 e^{\pi k f (h - h_{cr})t} \sin(\pi f t - \pi/4), \end{aligned} \tag{2}$$

where ξ_0 designates the initial wave amplitude and $h_{cr} \equiv \beta/(\pi k f)$, in which $\beta \equiv 2\nu k^2$. Equation (2) clearly shows that the single-mode Faraday waves excited carry a frequency equal to one-half of the drive frequency (f), namely, $\omega_k = \pi f$, and the corresponding wavelength (λ) and onset threshold (h_{cr}) are given as follows:

$$\lambda = 2\pi/k = 2\pi(\rho\omega_k^2/\sigma)^{-1/3} = 2\pi(\rho\pi^2 f^2/\sigma)^{-1/3} = (8\pi\sigma/\rho)^{1/3} f^{-2/3}. \tag{3}$$

$$h_{cr} \equiv \beta/(\pi k f) = 2\nu k/(\pi f) = 2\nu\rho^{1/3}(\pi\sigma)^{-1/3} f^{-1/3}. \tag{4}$$

Note that the onset threshold (h_{cr}) is at the minimum at the critical wave number (k_{cr}), i.e., the k^{th} mode Faraday wave in the aforementioned stability chart and also referred to in Eq. (1).

Dynamics of droplet ejection

Equation (4) shows the specific dependence of the onset threshold on the drive frequency (f) and the liquid properties (ρ, σ, and ν). It should be emphasized that h_{cr} decreases with the drive frequency in accordance with $f^{-1/3}$, and the wave amplitude $\xi_k(t)$ grows exponentially in time when $h > h_{cr}$. It is to be emphasized also that h_{cr} not only falls within the most unstable region but also decreases from 0.33 to 0.29 and to 0.24 μm, respectively, for water as an example, as f increases from 1.0 to 1.5 and to 2.5 MHz. The corresponding Faraday wavelengths are 12.2, 9.2, and 6.6 μm, and the respective wave numbers k_{cr}'s are 5204, 6820, and 9498 cm^{-1}. While h_{cr} decreases with the drive frequency in accordance with $f^{-1/3}$, the exponent $\pi k f(h - h_{cr})t$ in the exponential factor of $\xi_k(t)$ increases with the drive frequency in accordance with $f^{4/3}$. Thus, the temporal growth of the single-mode Faraday wave amplitude at MHz drive frequency is very rapid once the nozzle end face excitation displacement h exceeds the onset threshold h_{cr}. Take the Faraday waves at the 1.5 MHz drive frequency with the corresponding wavelength of 9.2 μm in water as an example, when h exceeds the predicted h_{cr} of 0.29 μm by as little as 0.01 μm the growth rate factor $e^{\pi k f(h-h_{cr})t}$ of the Faraday wave amplitude in Eq. (2) in a time increment of 0.5 ms is ~10^7 times that with $(h - h_{cr})$ as large as 100 μm at 200 Hz[25] drive frequency at the same time increment (0.5 ms). The amplitude growth rate factor at 1.5 MHz with $(h - h_{cr})$ of 0.01 μm in a time increment of 0.5 ms is still greater (by 8%) than that at 200 Hz with $(h - h_{cr})$ of 100 μm in a much longer time increment of 143 ms. When the wave amplitude grows and becomes too great to maintain wave stability, the Faraday waves break up, and thus droplets are ejected from the free surface of the liquid layer[31,32].

In summary, the scientific discovery on dynamics of droplet ejection at MHz drive frequency as described above together with the greatly magnified displacement on the end face of the MHz MFHUN enables generation of micrometer-size monodisperse droplets at low electrical drive power. This discovery also serves to explain the observations on atomization experiments at low drive frequencies described in "Introduction".

Size of ejected droplets

Now the ejected spherical droplets, with radius a and at the lowest oscillation mode frequency[33,35], are dispersed in air and free from external acceleration (g_e). Thus, by setting the frequency of the droplet's lowest oscillation mode equal to the nozzle drive frequency, the following theoretical droplet diameter ($D_p \equiv 2a$) in terms of Faraday wavelength (λ) is obtained:

$$D_p = 2(2/\pi^2)^{1/3}(\sigma/\rho)^{1/3} f^{-2/3} = 0.40\lambda. \tag{5}$$

Namely, the predicted droplet diameter equals four tenths of the Faraday wavelength involved. Note that this is the first theoretical formula for the droplet diameter in capillary wave-based ultrasonic droplet ejection. Clearly, for a given liquid to be nebulized, the desired size of the droplets can be controlled by the drive frequency (f) of the MFHUN in accordance with $f^{-2/3}$; the smaller the droplet size the higher the nozzle drive frequency.

Design, simulation, fabrication, characterization of MFHUNs, and droplet ejection studies

Design and simulation of MFHUNs

The innovation of the new ultrasonic delivery device lies in the multiple Fourier horns in cascade that vibrate in a single longitudinal mode along the nozzle axis at the same and single resonance frequency. As shown in **Fig. 2B**, the nozzle consists of a drive section and a resonator section. A lead zirconate titanate (PZT) piezoelectric transducer is bonded on the drive section to excite mechanical vibrations along the nozzle axis (Z-axis). The resonator section is made of multiple (3 in the example) Fourier horns in cascade[36]. The nozzle is designed to vibrate at the resonance frequency of the multiple Fourier horns. The resultant vibration amplitude (displacement) on the nozzle end face (tip of the distal horn) is greatly magnified with a gain of M^n for a n-Fourier horn nozzle with a magnification of M for each Fourier horn[15]. In order to produce

monodisperse droplets of desirable size range (2–5 μm) at high output rate and low electrical drive power (sub Watt), the optimum magnifications of 1.8 and 1.3 for the first three and the last horn of the 4-Fourier horn nozzles, respectively, were used in the design of optimized MFHUN.

Each Fourier horn is of half acoustic wavelength design[36,37]. The longitudinal axis of the nozzle (Z-axis) is in the direction of the primary flat, namely, <110> of the silicon wafer with the highest longitudinal acoustic velocity. A three-dimensional (3-D) finite element method (FEM) simulation is carried out using the commercial ANSYS (ANSYS Inc., Canonsburg, PA) Program first for vibration mode shape analysis and then for electrical impedance analysis[36]. The mode shape analysis determines the nozzle resonance frequency of pure longitudinal vibration mode; the electrical impedance analysis determines the longitudinal vibration displacement on the nozzle end face and the impedance at the nozzle resonance frequency. The resultant longitudinal vibration displacement on the nozzle end face is then used to determine the threshold voltage required to produce the onset threshold (h_{cr}) given by Eq. (4) in the first section of "Methods and Results". The threshold voltage thus obtained together with the resistive part of the impedance is then used to calculate the electrical drive power required for droplet ejection. Both the simulation results with the acoustical and electrical losses taken into account and the experimental results show that the optimum number of Fourier horns (n) in terms of electrical drive power requirement is 3 or 4. Due to the design of the nozzle, the onset threshold (h_{cr}) cannot be reached at any frequency outside the bandwidth (<10 kHz) of the designed resonance frequency; this design feature is critical to producing monodisperse droplets of the desired diameter at very low drive power.

The greatly enhanced peak vibration displacement (h) on the nozzle end face of the MFHUN facilitates the onset threshold required for initiation of temporal instability of the Faraday waves on the surface of the liquid layer and subsequent ejection of droplets at low electrical drive.

Fabrication and characterization of MFHUNs

The silicon-based MFHUNs of various designs in terms of the drive (resonance) frequency and the number of Fourier horns in cascade were fabricated using micro-electromechanical system (MEMS) technology.[38] The drive and resonator sections of the MFHUN were formed in a single-fabrication step using an inductive coupled plasma (ICP) process[39]. Note that a large number of nozzles with identical or different design specifications can be fabricated in one batch in a common silicon wafer. **Figure 3A** shows the layout of a large number of nozzles. After bonding of the PZT plate and the connecting wires, the resulting centimeter-size nozzles with optimum designs are shown in **Fig. 3B**.

The only essential characterization of the fabricated nozzle prior to droplet ejection experiments is to measure the impedance curve using Agilent impedance analyzer model 4294 A[15] from which the drive frequency and the electrical drive power are determined.

Droplet ejection studies

All the droplet ejection (atomization) experiments presented below were conducted using either the established bench-scale setup[16] or the pocket-size nebulizer. Major components of the setup are: (i) a PZT transducer drive system to provide a MHz electrical drive to the ultrasonic nozzle, (ii) a Syringe Pump (*kd* Scientific Model #101) to provide a controlled flow rate of liquid, (iii) a CCD camera to take pictures or movies of the droplets produced, and (iv) a Malvern/Spraytec System (Model #STP 5311) for analysis of the size distribution of the droplets.

Figures 4A and **4B** show photos of a stream of droplets produced from a water layer resting on the nozzle end face of the MHz nozzles using a high-resolution high-speed camera system with back-lighting and a normal speed camera system with front lighting, respectively. The droplet rates for the outputs of 40 and 350 μL/min (set by external feeding of water) are 1.4×10^7 and 4.0×10^8 droplets/sec, respectively. These high droplet output rates are in contrast to the continuous ink-jet printing

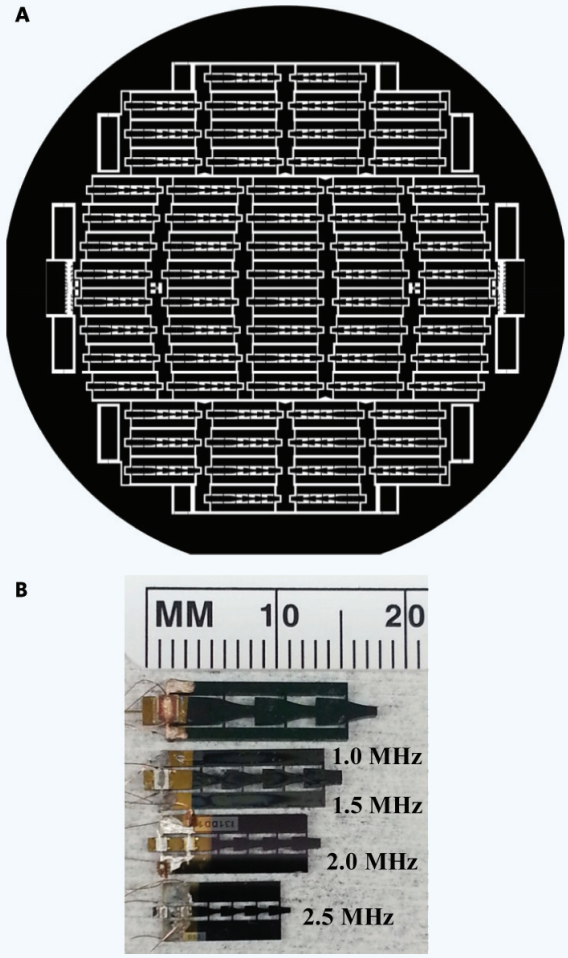

Figure 3 (**A**) Layout of nozzles with various designs in a common silicon wafer. (**B**) 1.0, 1.5, 2.0, and 2.5 MHz nozzles fabricated and studied.

(<10^6 droplets/sec (10 μm in diameter)[40]) resulting from the Rayleigh-Plateau instability. The short depth of focus provided by the high-resolution high-speed camera system enabled visualization of individual droplets ejected from the liquid layer and the thin-lighted curve caused by the Faraday waves excited on its surface as shown in **Fig. 4A**. The wavy liquid surface caused by the Faraday waves acts like optical gratings to scatter the incident light. Note that light scattered by Faraday waves excited on the liquid surface also resulted in intense brightness over the entire spherical surface of a water ball[32] (see **Fig. 2a** of Ref. 32) ejecting micro droplets.

The Malvern/Spraytec System is used to analyze the size distribution of droplets of **Fig. 4B**. The system is a non-invasive particle sizing instrument based on laser light diffraction. Since the laser beam had a cross sectional area (1 cm in diameter) much larger than the stream (spray) of droplets (~0.07×0.1 cm^2) produced by the nozzles, the data reported in this study were obtained from the entire cross-section of the droplet stream. The data include mass median diameter (MMD) and geometrical standard deviation (GSD). GSD and geometric mean of a data set with a log-normal distribution are, respectively, equivalent to the standard deviation and arithmetic mean of a data set with normal distribution. GSD is simply calculated by the geometric mean of quotients (ratios) D_{84}/D_{50} and D_{50}/D_{16}, where D_{84}, D_{50}, and D_{16} are, respectively, the droplet diameters at 84.1%, 50.0%, and 15.9% of the cumulative undersize percent of the droplet size distribution as shown in **Fig. 1B**. Note that the GSD was determined by least square fit ($R^2 = 0.9987$) of

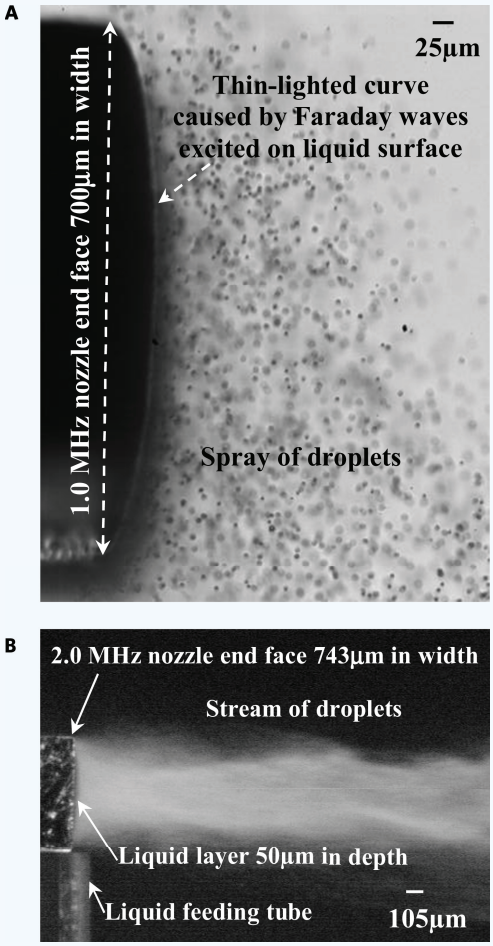

Figure 4 Stream of droplets ejected from the liquid layer resting on the end face of the nozzle tip: (**A**) High-speed photograph (10^4 frame/sec, Vision Research Model Phantom® v7.2) with short depth of focus for droplets stream at output rate of 40 μL/min with 1.0 MHz nozzle. (**B**) CCD image (20 frame/sec) of droplets stream at output rate of 350 μL/min and electrical drive power of 0.27 W with optimized 2.0 MHz nozzle. Note that the scale bars in (**A**) and (**B**) are 25 μm and 105 μm, respectively.

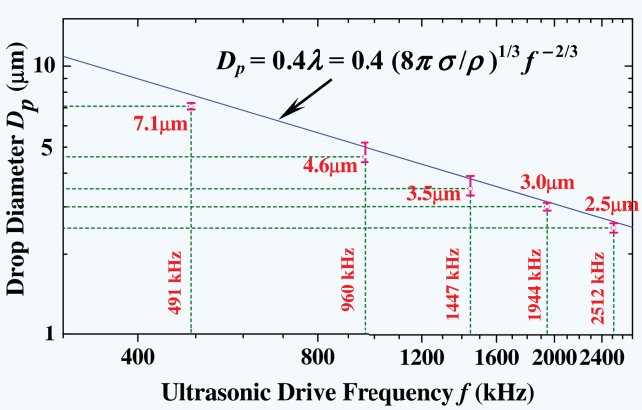

Figure 5 Comparison between the measured droplet diameters and the theoretical predictions.

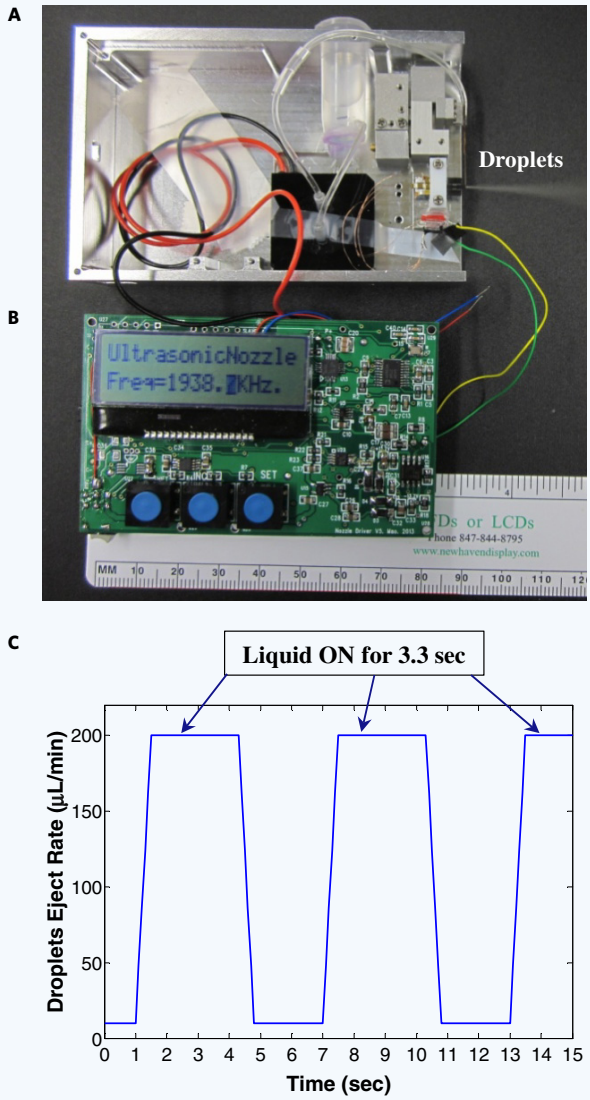

Figure 6 Pocket-size silicon-based ultrasonic nebulizer (8.8 cm × 5.9 cm × 1.9 cm): (**A**) Layout of ultrasonic nozzle and other mechanical components. (**B**) Layout of battery-powered electronic driver. (**C**) Externally actuated ON/OFF nebulization using a Harvard ventilator at 55% inspiratory, 750 mL tidal volume, and 10 breaths/min.

the cumulative undersize percentage curve obtained using the Malvern/Spraytec System. **Figure 5** shows clearly the excellent agreement between the measured droplet diameter and the theoretical prediction of Eq. (5) given in the first section of "Methods and Results".

Pocket-size ultrasonic nebulizer and nebulization of common drugs

As presented in the last subsection, the droplet ejection (atomization) experiments using the bench-scale unit with a single nozzle have demonstrated the capability of the silicon-based MHz MFHUNs for production of monodisperse droplets of desirable size (2 to 5 μm) and moderate output (up to 0.2 mL/min) at low electrical drive power (sub Watt). At the typical output rate of 0.15 mL/min with 3.5 μm-diameter droplets, which equals 1.1×10^8 droplets/sec, the required electrical drive power of 0.27 W corresponds to 2.4 nano joule per droplet generated. The centimeter-size nozzles with the low electrical power requirement

Table 1 Summary of drugs nebulized.

Medicine	Medicine concentration	Ultrasonic drive freq. (MHz)	Nebulizer unit	Droplet diameter (μm)	Output rate (μL/min)	Disease
Albuterol	25 mg/ml	1.0	Bench-scale	4.5	150	Asthma
Humulin, U100	100 units/ml	1.0	Bench-scale	4.5	100	Diabetes
Cobinamide[a]	100 mM	1.5	Pocket-size	3.9	130	Cyanide poisoning
Interferon-γ[b]	100 μg/0.5 ml	2.0	Pocket-size	2.9	100	Pulmonary fibrosis
Budesonide suspension	0.5 mg/2.0 ml	2.0	Pocket-size	3.1	350	Asthma

[a,b]Provided by Prof. G. Boss at UC San Diego and Prof. G.C. Smaldone, State Univ. of New York, Stony Brook, respectively.

enabled most recent realization of the first pocket-size ultrasonic nebulizer ($8.6 \times 5.6 \times 1.5$ cm^3). The nebulizer contains a single ultrasonic nozzle with optimum design as shown in **Fig. 3B**, IC electronic driver, battery, micro pump, drug reservoir, and liquid feed tube. The layout of the nozzle with other mechanical components and that of the battery-powered electronic driver are shown in **Figs. 6A** and **6B**, respectively. A range of drug substances for asthma, diabetes, pulmonary fibrosis, cyanide poisoning, etc. such as albuterol (salbutamol), Humulin U-100,[41] cobinamide, interferon-γ[10] and budesonide suspension[42] have been nebulized using the pocket-size nebulizer with desirable aerosol size and output rate as summarized in **Table 1**. Some drugs such as albuterol and cobinamide, and aqueous glycerol were successfully nebulized using the bench scale and/or the pocket-size units at varying concentrations with the corresponding range of viscosity up to as high as 4.5 cP and flow rate up to 350 μL/min. Furthermore, the pocket-size nebulizer has demonstrated its capability for nebulization of commercial budesonide suspension medicine that none of the current commercial ultrasonic nebulizers is capable of. It is to be noted that the demonstrated moderate output rate of 100–350 μL/min by the pocket-size unit would provide a higher effective dosage over the current commercial nebulizers in light of the higher aerosol monodispersity produced by the former. Clearly, a higher output rate can be accomplished readily by using an array of identical ultrasonic nozzles.

Breath actuation is an important operational requirement of a nebulizer in order to save the often expensive medicine. As shown in **Fig. 6C**, nebulization of medicine is turned ON/OFF by turning ON/OFF the feeding of the medicine using a piezoelectric micro pump to the nozzle end face in synchronization with the inspiratory cycle of a ventilator (Harvard piston pump). Specifically, a probe senses the UP/DOWN movement of the piston pump and sends a corresponding electrical signal to turn ON/OFF the liquid feed. A pressure sensor, with or without an ON/OFF disk/membrane valve, can be used for breathing without a ventilator. Thus, the pocket-size ultrasonic nebulizer is also capable of fulfilling this operational requirement.

DISCUSSION

Recently, we mimicked the Faraday's classical planar geometry of **Fig. 2A** using the end face of silicon-based MHz multiple-Fourier horn ultrasonic nozzle (MFHUN) and carried out theoretical and experimental studies at much higher drive frequencies (0.5 to 2.5 MHz)[15,16,31,32]. The resonance effect among the multiple Fourier horns designed for the single vibration mode at the single resonance frequency greatly magnifies the vibration displacement of the nozzle end face (by a factor of 2^n, where n designates the number of Fourier horns each with a magnification of 2) and, hence, readily facilitates formation and subsequent high-rate growth of Faraday waves on the free surface of the liquid layer. The single-mode Faraday wave excitation and amplification leads to generation of monodisperse droplets of desirable size range (~2 to 5 μm) at very low electrical drive power (<1 W)[16]. Such Faraday instability-based droplet ejection device is in stark contrast to all other existing ultrasonic devices employing a vibrating piezoelectric plate that simultaneously involve various droplet ejection mechanisms such as cavitation, impinging, and jetting in addition to capillary wave mechanism[25,43,44]. These ejection mechanisms require much higher electrical drive power (by 1 to 2 orders of magnitude) and produce broad droplet size distribution. The low electrical drive power requirement for the new ultrasonic device reported here not only facilitates miniaturization, but also minimizes temperature rises that might damage the medications to be aerosolized.

The precise control of particle size and much narrower particle size distribution achieved by the new device will improve targeting of treatment within the respiratory tract and improve delivery efficiency, resulting in better efficacy, fewer side effects, shorter treatment times, and lower medication costs compared with existing nebulizers. Additionally, high output rate of medicinal aerosol is desirable because it will shorten treatment times. The new device with a single nozzle alone has demonstrated an output rate up to 350 μL/min. Clearly, the output rate can be readily increased by using an array of identical nozzles. Furthermore, nozzle arrays with individual nozzles designed at different resonance frequency will provide the unique capability for production and mixing of aerosols of different sizes and/or medicines. Such nozzle arrays will provide a unique platform for basic research. The MEMS-based fabrication technology involved will enable construction of nozzle arrays of various designs.

The micron-size monodisperse droplets produced by the miniaturized low-power ultrasonic nozzles reported here may find a wide range of attractive applications other than inhalation drug delivery. Some examples of such applications include synthesis of nano particles via spray pyrolysis, sample injection in chemical analysis (e.g. mass spectroscopy), high-quality thin-film coating,[45] 3-D photoresist coating of micro- and nano-structures in fabrication of nano-electronic and -photonic devices, fuel injection in combustion, delivery of lipid-based micro-encapsulated biological entities or gene,[46,47] pharmaceutical preparation such as double emulsion,[48,49] rapid heat removal in laser surgery, and rapid administration of cosmetics.

The work reported here is the result of an interesting cross-fertilization between science and technology. Our original quest for an atomizer capable of producing micron-size monodisperse droplets led to the invention of the silicon-based MHz multiple Fourier horns in cascade. Subsequently, the study of the underlying mechanisms for droplet ejection led all the way back to Faraday's 1831 classical experiments involving a water layer at the very low drive frequency of 5 Hz and to many subsequent theoretical and experimental studies, but still at low drive frequencies up to ten's kHz. Our theoretical study on Faraday waves at the much higher drive frequency of MHz uncovered the frequency-sensitive dynamics of droplet ejection. The multiple-Fourier horn ultrasonic nozzle provides experimental verification of the theoretical predictions and facilitates the production of monodisperse droplets of desirable micron-size range at low drive power. Despite more than 180 years of continued interest and studies on Faraday waves it was only through our invention and realization of MHz ultrasonic nozzles with multiple Fourier horns in resonance that the technical potential of Faraday waves at MHz frequency range was discovered and led to a technology with immediate and important medical applications.

ACKNOWLEDGEMENTS

This work was supported by grants from the US National Institute of Health (NIH) NIBIB Grant #5R21EB006366, Counter ACT Program U54-NS063718 and AMRMC W81XWH-12-2-0114, Academia Sinica

and National Science Council, Taiwan, and Shih-Lin Electric USA. C.S. Tsai and S.C. Tsai would like to acknowledge collaborations with Matthew Brenner of UC Irvine, Gerry R. Boss of UC San Diego, and Steven Patterson of Univ. of Minnesota; encouragement and helpful discussions with Gerald C. Smaldone, State Univ. of New York, Stony Brook, NY, Howard A. Stone of Princeton University, Kwang-Jin Kim at Univ. of Southern California, Theodore Y.T. Wu of California Institute of Technology, Robert Langar of MIT, and Enrique Cerda at Univ. de Santiago de Chile. The authors also acknowledge Professor Peter Taborek and graduate student Serah Gutman of the Department of Physics and Astronomy at UC Irvine for loaning of their high-speed high-resolution camera and assistance in obtaining Fig. 4A, and the Institute of Physics, Academia Sinica, Taiwan for fabrication of some of the nozzle platforms.

AUTHOR CONTRIBUTIONS

C.S. Tsai initiated, acquired funding and supervised the study, and wrote the paper. S.C. Tsai and C.S. Tsai co-invented the device and developed the theory. S.C. Tsai also analyzed the experimental data and compared them with the theoretical predictions. R.W. Mao made major contributions to fabrication and construction of the device, and obtained the experimental data using the pocket-size nebulizer with the assistances of S.K. Lin and Y. Zhu. S.K. Lin also obtained the experimental data using the bench-scale setup.

COMPETING INTERESTS STATEMENT

The authors declare that they have no competing interests.

REFERENCES

1. Langer, R. Perspectives: Drug delivery — Drugs on target. *Science* **293**, 58–59 (2001).
2. Heyder, J. Deposition of inhaled particles in the human respiratory tract and consequences for regional targeting in respiratory drug delivery. *Proc. Am. Thorac. Soc.* **1**, 315–320 (2004).
3. Usmani, O.S., Biddiscombe, M.F. & Barnes, P.J. Regional lung deposition and bronchodilator response as a function of beta2-agonist particle size. *Am. J. Respir. Crit. Care Med.* **172**, 1497–1504 (2005).
4. Scheuch, G., Kohlhaeufl, M.J., Brand, P. & Siekmeier, R. Clinical perspectives on pulmonary systemic and macromolecular delivery. *Adv. Drug Deliv. Rev.* **58**, 996–1008 (2006).
5. Patton, J.S. & Byron, P.R. Inhaling medicines: Delivering drugs to the body through the lungs. *Nat. Rev. Drug Discovery* **6**, 67–74 (2007).
6. Sangwan, S., Condos, R. & Smaldone, G.C. Lung deposition and respirable mass during wet nebulization. *J. Aerosol. Med.* **16**, 379–386 (2003).
7. Watts, A.B., McConville, J.T. & Williams, R.O. 3rd. Current therapies and technological advances in aqueous aerosol drug delivery. *Drug Dev. Ind. Pharm.* **34**, 913–922 (2008).
8. Coates, A.L., Green, M., Leung, K., Chan, J., Ribeiro, N., Louca, E., Ratjen, F., Charron, M., Tservistas, M. & Keller, M. Rapid pulmonary delivery of inhaled tobramycin for Pseudomonas infection in cystic fibrosis: A pilot project. *Pediatr. Pulmonol.* **43**, 753–759 (2008).
9. Geller, D.E. & Kesser, K.C. The I-neb adaptive aerosol delivery system enhances delivery of alpha 1-antitrypsin with controlled inhalation. *J. Aerosol Med. Pulm. D* **23**, S55–S59 (2010).
10. Diaz, K.T., Skaria, S., Harris, K., Solomita, M., Lau, S., Bauer, K., Smaldone, G.C. & Condos, R. Delivery and safety of inhaled interferon-gamma in idiopathic pulmonary fibrosis. *J. Aerosol Med. Pulm. Drug Deliv.* **25**, 79–87 (2012).
11. Lass, J.S., Sant, A. & Knoch, M. New advances in aerosolised drug delivery: Vibrating membrane nebuliser technology. *Expert Opin. Drug Deliv.* **3**, 693–702 (2006).
12. Rottier, B.L., van Erp, C.J.P., Sluyter, T.S., Heijerman, H.G.M., Frijlink, H.W. & de Boer, A.H. Changes in performance of the Pari eFlow (R) Rapid and Pari LC Plus (TM) during 6 months use by CF patients. *J. Aerosol Med. Pulm. D* **22**, 263–269 (2009).
13. Kreuter, K.A., Lee, J., Mahon, S.B., Kim, J.G., Mukai, D., Mohammad, O., Blackledge, W., Boss, G.R., Tromberg, B.J. & Brenner, M. Rapid reversal of cyanide toxicity using a novel agent, cobinamide, assessed noninvasively using diffuse optical spectroscopy. *Chest* **134**, 124001 (2008).
14. Tsai, C.S., Mao, R.W., Zhu, Y., Chien, E., Tsai, S.C., Brenner, M., Mahon, S., Mukai, D., Lee, J., Yoon, D., Berney, T., Boss, G.R. & Patterson, S. Hand-held high-throughput ultrasonic monodisperse aerosol inhalers for detoxification of massive cyanide poisoning. *2012 IEEE Int. Ultrason. Symp. Proc.*, pp. 1632–1634 (2012).
15. Tsai, S.C., Cheng, C.H., Wang, N., Song, Y.L., Lee, C.T. & Tsai, C.S. Silicon-based Megahertz ultrasonic nozzles for production of monodisperse micrometer-sized droplets. *IEEE Trans. Ultrason. Ferroelect. Freq. Control* **56**, 1968–1979 (2009).
16. Tsai, C.S., Mao, R.W., Lin, S.K., Wang, N. & Tsai, S.C. Miniaturized multiple Fourier-horn ultrasonic droplet generators for biomedical applications. *Lab Chip* **10**, 2733–2740 (2010).
17. Faraday, M. On a peculiar class of acoustical figures and on certain forms assumed by groups of particles upon vibrating elastic surfaces. *Philos. Trans. Roy. Soc. Lond.* **A52**, 299–340 (1831).
18. Rayleigh, B. On the crispation of fluid resting upon a vibrating support. *Philos. Mag.* **16**, 50–58 (1883).
19. Benjamin, T.B. & Ursell, F. The stability of the plane free surface of a liquid in vertical periodic motion. *Proc. Roy. Soc. Lond. A* **225**, 505–515 (1954).
20. Miles, J. & Henderson, D. Parametrically forced surface-waves. *Annu. Rev. Fluid Mech.* **22**, 143–165 (1990).
21. Guthart, G.S. & Wu, T.Y.T. Observation of a standing kink cross wave parametrically excited. *Proc. Roy. Soc. Lond. A* **434**, 435–440 (1991).
22. Kumar, K. Linear theory of Faraday instability in viscous liquids. *Proc. Roy. Soc. Lond. A* **452**, 1113–1126 (1996).
23. Cerda, E.A. & Tirapegui, E.L. Faraday's instability for viscous liquids. *Phys. Rev. Lett.* **78**, 859–862 (1997).
24. Sindayihebura, D. & Bolle, L. Ultrasonic atomization of liquids: Stability analysis of the viscous liquid film free surface. *Atomization Sprays* **8**, 217–233 (1998).
25. Yule, A.J. & Al-Suleimani, Y. On droplet formation from capillary waves on a vibrating surface. *Proc. Roy. Soc. Lond. A* **456**, 1069–1085 (2000).
26. Ubal, S., Giavedoni, M.D. & Saita, F.A. A numerical analysis of the influence of the liquid depth on two dimensional Faraday waves. *Phys. Fluids* **15**, 3099–3113 (2003).
27. James, A.J., Vukasinovic, B., Smith, M.K. & Glezer, A. Vibration-induced drop atomization and bursting. *J. Fluid Mech.* **476**, 1–28 (2003).
28. Wright, P.H. & Saylor, J.R. Patterning of particulate films using Faraday waves. *Rev. Sci. Instrum.* **74**, 4063–4070 (2003).
29. Shats, M., Xia, H. & Punzmann, H. Parametrically excited water surface ripples as ensembles of oscillons. *Phys. Rev. Lett.* **108**, 034502–034501 to 034505 (2012).
30. Edwards, W.S. & Fauve, S. Parametrically excited quasi-crystalline surface-waves. *Phys. Rev. E* **47**, R788–R791 (1993).
31. Tsai, S.C. & Tsai, C.S. Linear theory of temporal instability of Megahertz Faraday waves for monodisperse microdroplet ejection. *IEEE Trans. Ultrason. Ferroelect. Freq. Control* **60**, 1746–1754 (2013).
32. Tsai, S.C., Lin, S.K., Mao, R.W. & Tsai, C.S. Ejection of uniform micrometer-sized droplets from Faraday waves on a millimeter-sized water drop. *Phys. Rev. Lett.* **108**, 154501–154501 to 154505 (2012).
33. Landau, L.D. & Lifshitz, E.M. *Fluid Mechanics*. Elsevier Publishing, London/New York (1987).
34. Cerda, E.A. & Tirapegui, E.L. Faraday's instability in viscous fluid. *J. Fluid Mech.* **368**, 195–228 (1998).
35. Rayleigh, B. On the capillary phenomenon of jets. *Proc. Roy. Soc. Lond.* **29**, 71–97 (1879).
36. Tsai, S.C., Song, Y.L., Tseng, T.K., Chou, Y.F., Chen, W.J. & Tsai, C.S. High-frequency silicon-based ultrasonic nozzles using multiple Fourier horns. *IEEE Trans. Ultrason. Ferroelectr. Freq. Control* **51**, 277–285 (2004).
37. Tsai, S.C., Song, Y.L., Tsai, C.S., Chou, Y.F. & Cheng, C.H. Ultrasonic atomization using MHz silicon-based multiple-Fourier horn nozzles. *Appl. Phys. Lett.* **88**, 014102–014101 (2006).
38. Lal, A. & White, R.M. Micromachined silicon ultrasonic atomizer. *IEEE Int. Ultrason. Symp. Proc.*, pp. 339–342 (1996).
39. McAuley, S.A., Ashraf, H., Atabo, L., Chambers, A., Hall, S., Hopkins, J. & Nicholls, G. Silicon micromachining using a high-density plasma source. *J. Phys. D* **34**, 2769–2774 (2001).
40. Hertz, C.H. & Samuelsson, B.A. Ink jet printing of high quality color images. *J. Imag. Tech.* **15**, 141–148 (1989).
41. Tsai, S.C., Mao, R.W., Mukai, D., Lin, S.K., Wilson, A.F., Wang, N., Brenner, M., George, S.C., Yang, J.Y., Wang, P. & Tsai, C.S. Pulmonary drug delivery using miniaturized silicon-based MHz ultrasonic nozzles. Presented at the *Int. Conf. Accelerating Biopharm. Dev.*, Colorado, 9–12 March (2009).
42. Nikander, K., Turpeinen, M. & Wollmer, P. The conventional ultrasonic nebulizer proved inefficient in nebulizing a suspension. *J. Aerosol Med.* **12**, 47–53 (1999).
43. Maehara, N., Ueha, S. & Mori, E. Influence of the vibrating system of a multipinhole-plate ultrasonic nebulizer on its performance. *Rev. Sci. Instrum.* **57**, 2870–2876 (1986).
44. Tsai, S.C., Luu, P., Childs, P., Teshome, A. & Tsai, C.S. The role of capillary waves in two-fluid atomization. *Phys. Fluids* **9**, 2909–2918 (1997).
45. Bird, J.C., Mandre, S & Stone, H.A. Coalescence of spreading droplets on a wettable substrate. *Phys. Rev. Lett.* **97**, 064501-064501 to 064504 (2006).
46. Dang, J.M. & Leong, K.W. Natural polymers for gene delivery and tissue engineering. *Adv. Drug Delivery Rev.* **58**, 487–499 (2006).
47. Zarnitsyn, V.G., Meacham, J.M., Varady, M.J., Hao, C.H., Degertekin, F.L. & Fedorov, A.G. Electrosonic ejector microarray for drug and gene delivery. *Biomed. Microdevices* **10**, 299–308 (2008).
48. Garstecki, P., Fuerstman, M.J., Stone, H.A. & Whitesides, G.M. Formation of droplets and bubbles in a microfluidic T-junction — Scaling and mechanism of break-up. *Lab Chip* **6**, 437–446 (2006).
49. Tan, Y.C. Hettiarachchi, K., Siu, M., Pan, Y.R. & Lee, A.P. Controlled microfluidic encapsulation of cells, proteins, and microbeads in lipid vesicles. *J. Am. Chem. Soc.* **128**, 5656–5658 (2006).